Final Draft
of the original manuscript:

Huang, Y.; Wang, Y.; Wan, L.; Liu, H.; Shen, J.; dos Santos, J.F.; Zhou, L.; Feng, J.:

Material-flow behavior during friction-stir welding of 6082-T6 aluminum alloy

In: The International Journal of Advanced Manufacturing Technology (2016) Springer

DOI: 10.1007/s00170-016-8603-7

Material Flow Behavior during Friction Stir Welding of 6082-T6 Aluminum Alloy

Yongxian Huang[a,b*], Yaobin Wang[a], Long Wan[a], Haoshu Liu[a], Junjun Shen[b], Jorge F. dos Santos[b], Li Zhou[a,c], Jicai Feng[a,c]

[a]State Key Laboratory of Advanced Welding and Joining, Harbin Institute of Technology, Harbin 150001, People's Republic of China

[b]Institute of Materials Research, Helmholtz-Zentrum Geesthacht, Geesthacht 21502, Germany

[c]Shandong Provincial Key Laboratory of Special Welding Technology, Harbin Institute of Technology at Weihai, Weihai 264209, People's Republic of China

Abstract Material flow behavior during friction stir welding of 6082-T6 aluminum alloy has been visualized by marker insert technique. An interesting pattern existed in welding nugget zone (WNZ). Four stacked layers were evolved in WNZ in the transverse section. The material flow behavior in vertical direction was detected by observing the distribution of Cu foil fragments and Al-Cu intermetallic compounds. The downward and upward flows encounter at the advancing side in material depositing process, changing the morphology of WNZ. A conceptual balanced flow model and a plastic material flow model were used to describe the material flow behavior, and the origin of the downward material flow in the advancing side was discussed. The study of material flow behavior is meaningful for optimizing the fabrication and performance of joint.

Keywords Friction stir welding · Aluminum alloy · Marker material · Material flow behavior · Welding nugget zone

1 Introduction

Friction stir welding (FSW) was invented by The Welding Institute (TWI) in 1991 [1]. As a relatively new solid state welding technique, it is widely applied in aluminum alloys especially which are difficult to weld by conventional fusion techniques [2]. The material flow in FSW process is related to the microstructure formation and has great influence on the properties of weld joints. Investigating

material flow behavior in FSW process is meaningful for optimizing process parameters, analyzing welding defects, and controlling microstructure and properties of welds. A series of investigations have been made to study the material flow during FSW. Special marker materials were widely used to mark material flow path since the process could not be observed directly. The phenomenon of simple extrusion and chaotic mixing was reported [3-5]. Colligan [3] used steel shots as marker and revealed stirring and extruding behavior in material flow. Guerra et al. [4] combined tracer technique with pin frozen technique and found that material on the advancing front side entered into the rotational zone around pin in which material was intensively deformed while material on the retreating front side was only extruded.

The same conclusion was also drawn by Kumar and Kailas [5]. They placed marker foil on faying surface and deviated the traveling path of the tool from the faying surface, which made the foil move from advancing side to retreating side with the advance of rotating tool. Some researches achieved the three-dimensional images of material flow by tracer technique, which facilitated the observation of material flow. Reynolds et al. [6] and Zhao [7] investigated the distribution of the marker in the top, middle and bottom positions of welds and combined these data into a three-dimensional map. Schmidt et al. [8] employed X-ray and computer tomography to study material flow with a thin marker foil in the workpiece and obtained two and three-dimensional CT images. Morisada et al. [9] observed the locus of the tungsten tracer by two pairs of X-ray transmission real-time imaging systems. A three-dimensional image was obtained and the material flow was clearly represented by the movement of the tracer. Xu et al. [10] investigated texture patterns on transverse, longitudinal and horizontal cross-sections, suggesting that the periodically spaced material regions may lead to the good correlation between texture patterns and equivalent plastic strain contours from simulations.

FSW of dissimilar materials were also widely applied to studying material flow behavior. Investigations of material flow by FSW of Al to Cu [11, 12], Al to Mg [13] and Al to steel [14] were reported. However, because of large physical differences between Al with other metals, it was better to study material flow through FSW of dissimilar Al alloys [15, 16]. Investigation of crystallographic texture was an interesting way to study material flow behavior. Fonda et al. [17] discovered a periodic variation in both texture and the orientation of that texture along the weld which was attributed to the oscillation of an off-centered tool. They suggested that such oscillation resulted in material periodically extruded or entrained from TMAZ

into WNZ during each revolution of the tool. Some researchers also reported that intense shear plastic flow near the pin surface greatly changed texture in WNZ [18, 19]. Currently, some consensuses about material flow have been reached. Material flow behavior was closely influenced by welding parameters [20] and the shape of welding tools [21-23]. During FSW process, the material ahead of welding tool is firstly heated and softened and then transferred from leading side to trailing side under the effect of rotating tool. Finally the material deposits in the trailing side to form weld seam. In the transfer process, the material driven effects of shoulder and pin were not similar and the concept of shoulder driven flow and pin driven flow were proposed [4, 24].

To better understand flow behavior, the plastic material flow model is needed. Nandan et al. [25] regarded viscoplastic material near the tool surface as non-Newtonian fluid and achieved three-dimensional calculations on the view of conservation of mass, momentum and energy. The computed material flow behavior and temperatures corresponded well with the corresponding experiments. Some models were also proposed to facilitate the comprehension of material flow behavior. Arbegast [26] investigated typical defect types in friction stir welds and proposed a conceptual flow-balanced model to discuss the flow conditions of defect formation. Li et al. [27] established a plastic material flow model to represent the flow behavior around rotating tool base on previous reports and their own experimental results. But detailed research about origins of material flow behavior was not given.

Despite plenty of work on these important aspects, some controversies still exist and material flow behavior during FSW is not fully understood. In the present work, 0.1-mm-thick Cu foils were placed as marker material at different positions of the faying surface between two 6082-T6 aluminum alloy plates. The distribution of Cu foil fragments and Al-Cu intermetallic compounds were analyzed to investigate the material flow behavior, especially how materials flow during the depositing process in the trailing side of the rotating tool, which directly influences the formation of the joint. A conceptual flow-balanced model and a plastic metal flow model were used to explain material flow behavior.

2 Experimental procedure

The materials used were 6082-T6 aluminum alloy plates (300 mm × 100 mm × 5 mm) and T3 Cu foils. The nominal chemical composition of 6082-T6 aluminum alloy and T3 Cu were listed in Table 1. The FSW process were finished using an FSW machine (FSW-3LM-003). The FSW tool was made of high speed tool steel with a

concave shoulder and a frustum-shaped and right-hand threaded pin. Concrete information of geometries and features of the tool were listed in Table 2. The Cu foils with 0.1 mm thickness and 2 mm width were placed in three different configurations, i.e., at the top part (‘C1’), middle part (‘C2’), and bottom part (‘C3’) of the sheet faying interface, as shown in Fig. 1. Two adjacent markers were staggered 2mm so that they would not be mixed together and flow modes in different heights of the joint could be distinguished. Cu foil can be easily fragmented into debris and flow along with parent material due to slight thickness.

The oxide film on aluminum sheets surface was removed and surface polishing was performed. The designed welding experiments (‘E1’ to ‘E7’) were listed in Table 3, in which placements of Cu foil and process conditions were described. The joints were sectioned along the vertical plane in welding direction. Metallographic sections were subjected to mechanical grinding and final polishing with a solution of 0.1 mm silica suspension. The specimens were etched with reagent (1 ml hydrofluoric acid + 1.5 ml hydrochloric acid + 2.5 ml nitric acid + 95 ml water) to reveal the macro and microstructures. The material flow and microstructure were observed by optical microscopy (OM, Olympus-MPG3). Al-Cu intermetallic compounds were detected and identified by scanning electron microscope (SEM, Quanta 200FEG) equipped with energy dispersive spectroscopy (EDS).

3 Results and Discussion

3.1 Morphology of WNZ

Fig. 2 showed a special and interesting pattern in the WNZ. Different from conventional ‘onion rings’ structure, the special pattern of WNZ consisted of four stacked layers. The four layers in WNZ were marked as layer I, II, III and IV from up to bottom. Although the formation of four stacked layers was not clear, multiple layers or onion rings structures stacked in vertical direction were reported [10, 15, 28]. Ouyang el al. [15] discovered a double-cell structure of onion rings in the dissimilar FSW of 6061-Al alloy to 2024-Al alloy plates. They ascribed it to the shortcut of return flow back to the surface instead of reaching the root of nugget. However, the stacked layers in the present study showed incomplete onion rings with banded structures mainly distributing in the advancing side instead of complete onion rings. It showed similar WNZ pattern in previous study of Xu and Deng [10]. They suggested that the banded texture patterns in WNZ had a strong relation with the equivalent plastic strain field in the welds. Guo et al. [28] observed distinct multiple stacked vortexes centers in WNZ. They attributed the formation of this pattern to the features

of the stir pin. To delineate the morphology of WNZ clearer and study material flow in FSW, marker material was added onto the faying surface at different positions. Rotation rates of 800 rpm and 1200 rpm were adopted and the macrographs of the cross sections were shown in Fig. 3. All cross sections of marked samples (Fig. 3a-f), showed four layers stacked in the vertical direction and each layer consisted of several concentric ellipses. The inner ellipses were complete while as progressed towards periphery, the ellipses became incomplete. Banded structures gathered in the advancing side and ellipses gradually disappeared in the retreating side. Looking into the gathered banded structures in the advancing side, it consisted of black lamellae and every band was alike with each other in the same layer. As progressed towards the boundary of WNZ, the space between two adjacent bands became narrow. It account for huge centrifugal force generated by the rotating pin pushing softened material to the boundary of 'extrude die', which corresponded to the in situ extrusion model proposed by Reynolds [6].

Fig. 4 showed that there was a quantity of second phase particles embedded in black lamellae. The EDS analysis results (scan area was framed) shown in Fig. 4b indicated that these particles mainly contain Al and Cu elements. According to previous study [12, 29-31], $Al_2Cu(\theta)$, $Al_4Cu_9(\gamma)$ and $AlCu(\eta)$ were common phases generated during Al-Cu dissimilar metal FSW. In the present experiment, Cu foils were placed in the middle of the welding path. Foils experienced large plastic deformation and thermal exposure. Because of thin thickness, they were easy to be fragmented and react with Al matrix. As peak temperature and huge plastic deformation were expected at the interface region between weld metal and rotating pin, Al-Cu intermetallic compounds began to form in this region. After generated, Al-Cu intermetallic compounds flowed with the plasticized material. The WNZ pattern of the weld without Cu foil (Fig. 2) showed four stacked layers consisted of black bands. As for WNZ patterns of the welds which added Cu foils (Fig. 3), the morphology of stacked layers did not change a lot but black Al-Cu intermetallic compounds filled in these bands. It suggested that the final deposited position of Al-Cu intermetallic compounds corresponded with the real material depositing behavior behind the pin, providing a visible convenience to investigate material flow.

3.2 Material flow behavior

In Fig. 3f, bands in layer II, III and IV got special figures. Every figure was a little different from the adjacent one in the same layer. However, with the increasing of the intervals, the difference became larger. As inferred above, material diffused toward the boundary. The transformation of these figures showed the evolution of

plasticized material when it diffused from the edge of pin to the boundary. Fig. 5a showed the magnification view of layer II and III indicated in Fig. 3f. As shown in Fig. 5a, segments (1), (2) and (3) belonged to layer II and segments (4) and (5) belonged to layer III. Segments in the same layer can be regarded as the transformation of one segment during the material extrusion process. Fig. 5b segregated these analogous segments in layer II and III. In Fig. 5b, every segment was divided into two parts, head and tail. For segments (1), (2) and (3), the bulgy head of (1) became circular in (2) then protruded downwards in (3) while the tail pointed downwards and became longer. In consideration of the centrifugal force caused by the rotating tool, the material flowed outwards every layer and the variation of (1), (2) and (3) revealed the downward material flow in layer II. In the same way, it could be postulated that the material flowed upwards in layer III.

The morphology of streamlines in thermal affected zone (TMAZ) verified this observation. Bent directions of streamlines in TMAZ indicated the material flow behavior in vertical direction [32]. As shown in Fig. 6, the red lines delineated the flow trend of streamlines. Streamlines of TMAZ in the advancing side bent downwards at upper part and upwards at lower part which showed the material flowed downwards at upper part and upwards at lower part. In addition, a special structure was framed by black box. The structure was a bulge of layer I or between layer I and II in the advancing side. Outside the bulge was the bent streamlines in TMAZ. According to bent directions of streamlines, it was clear that the upward and downward materials converged together. As a result, the bulge structure was formed at layer I or between layer I and II in the advancing side. Vertical material flow also influences the structure of WNZ. The thickness of layer I was measured by the minor axis of the outer ellipse. Fig. 7 showed the compression of layer I at the rotation rate of 1200 rpm compared with 800 rpm. As the rotation speed increased, material flowed more intensely [20]. Therefore the upward and downward forces both got strengthened which led to the compression of layer I.

3.3 Material Flow Model

It is clear that the use of Cu foil provides a good method to study material flow during FSW. The balanced flow model [26] was cited and optimized to explain the material flow behavior during FSW, as shown in Fig. 8. In the model, material flow was divided into four parts: shoulder driven flow, pin driven flow, flow in swirl zone under the pin and excess flow under the shoulder in the advancing side. During material transferring process from leading side to trailing side, Cu foils positioned at upper and bottom part experienced shoulder and pin driven flow respectively. Fig. 9

showed the view of the upper parts of Fig. 3a and b. Cu foil positioned at upper part was deformed and stretched in the shoulder driven flow and it finally deposited on the surface in the advancing side. Material in this zone was likely to be driven from the retreating side to the advancing side behind the tool in the depositing process. Bottom part was a position where Cu foil was only influenced by top half part of the pin and fragments indicated the material flow accurately. As shown in Fig. 10, Cu foil was deformed by the rotating pin and fragments only distributed in the retreating side. The morphology of fragments implied the material in retreating side flow upwards, which corresponded to the bent direction of grains in TMAZ. It could be postulated that Cu foil positioned at bottom part was more likely to be extruded and mainly deposited in the retreating side. The observation of Cu foil fragments in upper and bottom position verified the extruding and stirring behavior proposed by Colligan [3].

The onion rings (band structures) were formed due to the arc-shaped layers extruding and stacking behaviors by rotating tool, especially affected by the stirring pin [33, 34]. As shown in Fig. 11a, intervals of bands on transverse cross sections associated with rotation rate, welding speed and pin radius. As a result, weld pitch (tool advancement per revolution) could be calculated by intervals of bands. Intervals data in Fig. 2 were taken into calculation and shown in Fig. 11b with pin profile added. Distances between bands and centerlines in layer I and IV were listed in Table 4. According to Fig. 11a, the calculations of weld pitch were plotted in Fig. 12. The data of former bands were close to the true value of 0.25mm. However, with bands got far from centerline the calculations became larger. It may account for the extrusion behavior generated by the rotating pin, which pushed material outside. There was a convenient way to verify the layers extruding and stacking behaviors. Because bands in WNZ were generated by the stirring pin and intervals between adjacent two bands corresponded well with pin radius, the number of bands in the range of pin radius was equal to the quotient of dividing pin radius by weld pitch. The numbers of bands in the range of pin radius in layer I and layer IV were 9 and 7, close to the theoretical value of 10 and 8. Applying this method to the welds marked by Cu foils, the results matched well. Band structures in advancing side reflected the material extruding and stacking behavior in the trailing side of stir pin.

As discussed above, a majority of plasticized material was first extruded towards retreating side. Then in depositing process, shoulder driven flow drove material from the retreating side to the advancing side and pin driven flow caused material extruded and stacked layer by layer behind the pin. It was necessary to discuss material

transferring process from the leading side to the trailing side. To obtain sound welding joints, the mass of material flow per cycle (M^{PC}) should be equivalent to the mass of shoulder driven flow (M^{S}), pin driven flow (M^{P}), flow in swirl zone (M^{SW}) and excess flow (M^{EX}) (every mass was shown in Fig. 8). It can be present by Eq. 1 [35].

$$M^{PC} = M^{S} + M^{P} + M^{SW} + M^{EX} (M^{EX} = M^{EX}_{Balanced}) \quad [1]$$

It should be noticed that M^{EX} was different from Reference [26] and [35]. In Reference [26], there was no M^{EX} but M_{T}^{XS} which was defined as excess material around the pin and beneath the shoulder. In Reference [35], M^{EX} meant the mass of material flow in the excess zone besides the pin driven zone. In this paper, M^{EX} was only the excess flow under the shoulder in the advancing side, which dominated the excess flow in the whole weld zone.

The flow balanced model suggested three states of material flow. They were insufficient, balanced and excess material flow states which were greatly affected by M^{EX}. The equation of balanced state was given above and another two states could be represented as follows:

$$M^{PC} > M^{S} + M^{P} + M^{SW} + M^{EX} (M^{EX} = M^{EX}_{Insufficient}) \quad [2]$$

$$M^{PC} < M^{S} + M^{P} + M^{SW} + M^{EX} (M^{EX} = M^{EX}_{Excess}) \quad [3]$$

According to Eqs. 1-3, M^{EX} was critical to determine the state of material flow, which could furthermore affect the quality of welding joints. M^{EX} of insufficient and excess flow states deteriorated welding joints of FSW. As $M^{EX} < M^{EX}_{Balanced} (M^{EX} = M^{EX}_{Insufficient})$, volumetric formation would be developed such as wormhole in advancing side. On the condition of $M^{EX} > M^{EX}_{Balanced} (M^{EX} = M^{EX}_{Excess})$, superabundant M^{EX} could collapse the nugget. These two defects always existed in the advancing side of WNZ, which have been shown in Reference [24, 26]. It could be postulated that M^{EX} mainly influenced the formation of WNZ in the advancing side.

The excess material flow (M^{EX}) was mainly generated by the tilting tool. During the process of FSW, an angle of tool axis tilting with respect to the normal of workpiece surface was often exerted. A proper tilt angle of tool towards trailing side made the shoulder hold the stirred material and move material from leading side to trailing side efficiently. Li et al. [27] proposed a plastic material flow model in FSW based on their experiment results and previous reports, which clearly showed different

flow mode in vertical direction and the generation of excess material flow. Fig. 13 showed a model to further explain the generation of excess material flow. In this model, the tilting shoulder connected closely with workpiece generating an obliquely downward force. The force could be decomposed into a forward force and a downward force (Fig. 13a). The forward force contributed to drive the stirred material into the concave of the shoulder, which helped to eliminate the flash formation and made the surface of welds elegant. The downward force combined with the driven flow of rotating shoulder drove the plastic material flow downward into WNZ in the advancing side. In the present experiment, right-hand threaded pin combined with counterclockwise rotation drove material close to the pin surface downwards, forming the ring vortex flow as shown in Fig. 13a. The downward material flow encountered the upward material flow subsequently, in which the upward material flow shown in Fig. 13a was a part of ring vortex flow [36, 37]. It attributed to the generation of the bulge structure of layer I or between layer I and II in the advancing side (Fig. 6) and the compression of layer I (Fig. 7) in material depositing process. In the area of the trailing advancing side beneath the shoulder, material flow of each material point interacted with each other (Fig. 13b). Convergence of material flow in this region drove more material to flow downward, which strengthened the downward material flow and accelerated the substantial transportation. Despite of the deviation from balanced model [26], M^{EX} can be represented as:

$$M^{EX} = \psi(\alpha, \beta, \varphi^2) \qquad [4]$$

M^{EX} was represented by a function in which the boundary condition factor ψ was determined by thermal and mechanical properties of material around the pin and beneath the shoulder. In Eq. 4, α and β were the tool shape factor of pin and shoulder, and $\varphi = \omega / v$ (ω represented the rotation rate and v represented the welding speed) was the processing parameter factor. It was obvious that the shape of the tool and welding parameters influence the amount of excess material flow.

4 Conclusions

The Cu foil as marker material was used to study the material flow behavior of 6082-T6 Aluminum alloy in FSW by observing the distribution and morphology of fragile Cu foil and Al-Cu intermetallic compounds. It was observed that shoulder driven flow drove material from retreating side to advancing side and pin driven flow mainly extruded material to the retreating side. In advancing side, flow collision in

vertical direction was detected by observing flow pattern in layer II and III and it cased bulge structure in advancing side and compression of layer I. The excess material flow played an important role in this flow collision and it was proved to derive from the tilt angle of welding tool and influenced greatly by the shape of the tool and welding parameters. Through flow balanced model, shoulder driven flow, pin driven flow and excess material flow were integrated to provide a conceptual cognition of the material flow behavior in WNZ. It verified that excess material flow is a crucial factor of the weld formation.

Acknowledgements The work was supported by the National Natural Science Foundation of China (No. 51575132).

Tables

Table 1 Chemical compositions of 6082-T6 aluminum alloy and T3 Cu foil (wt.%)

Material	Al	Cu+Ag	Mg	Fe	Cr	Si	Mn	Zn	Ni
T3	—	Bal.	—	0.043	—	—	—	—	0.2
6082-T6	Bal.	0.10	1.1	0.50	0.25	0.90	0.70	0.20	—

Table 2 Welding tool geometries and features for FSW

Diameter of shoulder/mm	Length of pin /mm	Bottom diameter of pin/mm	Top diameter of pin/mm	Plunge depth /mm
15.00	4.64	6.10	3.50	0.20

Table 3 The instructions for the FSW experiment

Experiment design	Placement of Cu foil	Tool rotation rate /rpm	Welding speed /mm min^{-1}	Tilt angle /°
E 1	C1	800	200	2.5
E 2	C1	1200	200	2.5
E 3	C2	800	200	2.5
E 4	C2	1200	200	2.5
E 5	C3	800	200	2.5
E 6	C3	1200	200	2.5
E 7	none	800	200	2.5

Table 4 Distances between bands and centerline

Number of band	Band 1	Band 2	Band 3	Band 4	Band 5	Band 6	Band 7	Band 8	Pin radium
Layer I	0.74	1.29	1.63	1.88	2.06	2.22	2.36	2.47	2.52
Layer IV	0.99	1.31	1.56	1.75	1.91				1.98

Figure captions:

Fig. 1 Schematic illustrations of Cu foil positions. **a** side view. **b** top view.

Fig. 2 The transverse cross-sections of FSW joint without Cu foil.

Fig. 3 The transverse cross-sections of three different Cu foil positions in the rotation rate of 800 rpm and 1200 rpm. **a** C1/800 rpm. **b** C1/1200 rpm. **c** C2/800 rpm. **d** C2/1200 rpm. **e** C3/800 rpm. **f** C3/1200 rpm.

Fig. 4 Al-Cu intermetallic compounds in black lamellae in WNZ. **a** SEM image. **b** EDS spectrums.

Fig. 5 Material flow indicated by layer II and layer III pattern. **a** magnification view of layer II and III in Fig. 3f. **b** transformation of analogous figures.

Fig. 6 Bent directions of streamlines in TMAZ with the variation of the position of Cu foil. **a** upper part. **b** middle part. **c** bottom part.

Fig. 7 The comparison of the thickness of layer I in WNZ with different welding parameters. **a** C2/800rpm. **b** C1/1200rpm.

Fig. 8 Conceptual model of balanced flow.

Fig. 9 The deformed Cu foil distributes on the surface of welds in the advancing side when initially positioned at upper part. **a** 800 rpm. **b** 1200 rpm.

Fig. 10 The distribution and morphology of deposited Cu foil fragments with different welding parameters. **a** C3/800 rpm. **b** C3/1200 rpm.

Fig. 11 Schematic illustrations of the formation of band structures in the advancing side.

Fig. 12 Calculation of advancement per revolution in layer I and layer IV.

Fig. 13 Material flow in the weld beneath the shoulder. **a** vertical section. **b** cross section.

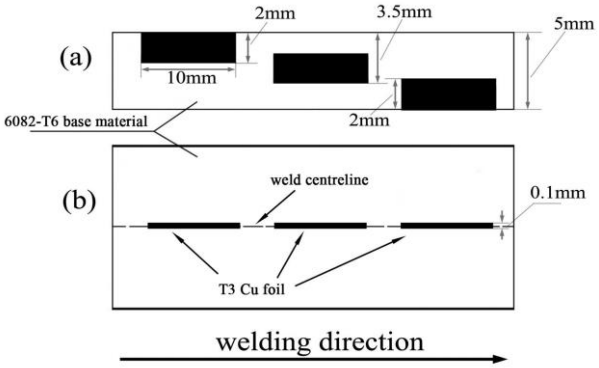

Figure 1

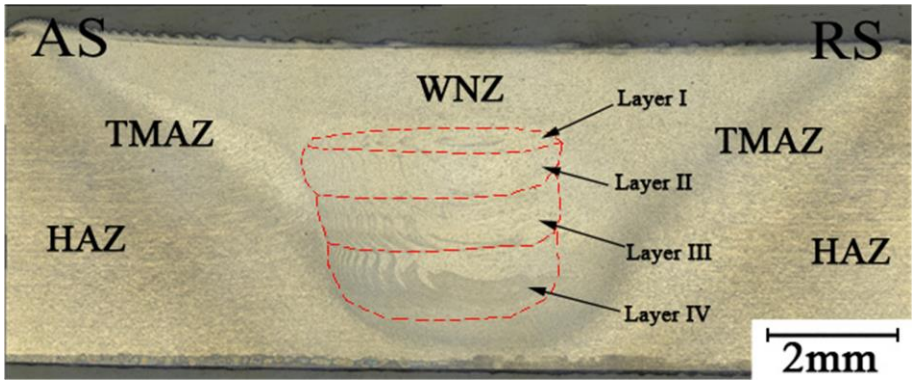

Figure 2

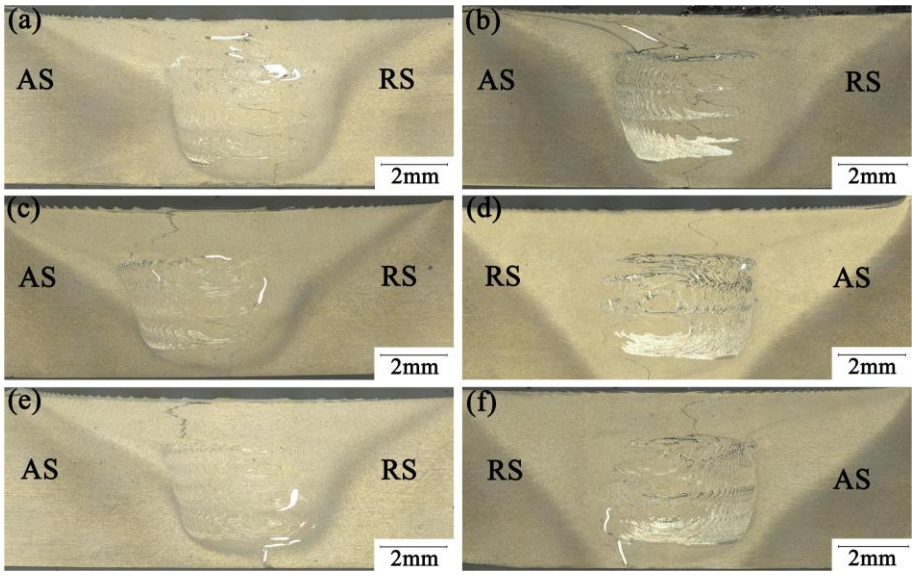

Figure 3

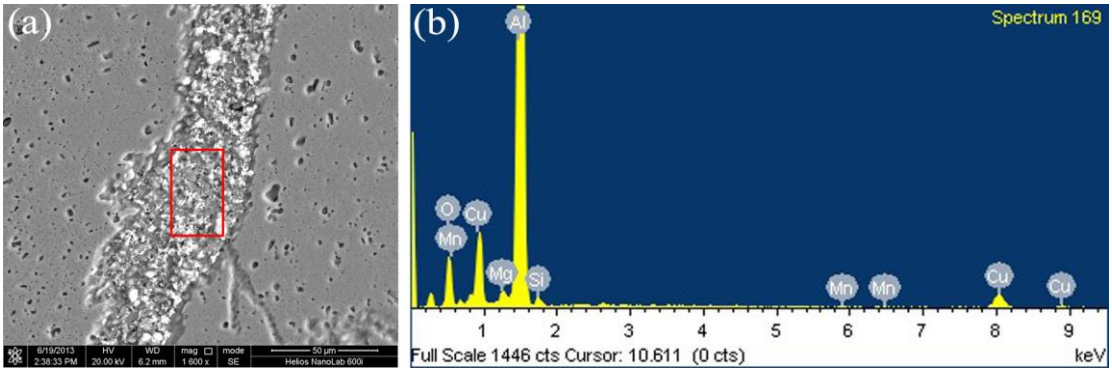

Figure 4

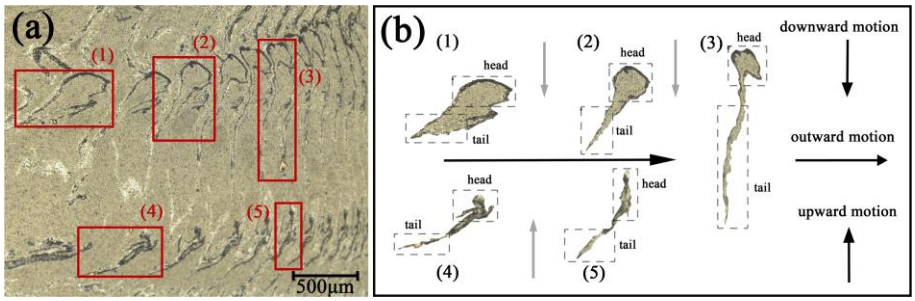

Figure 5

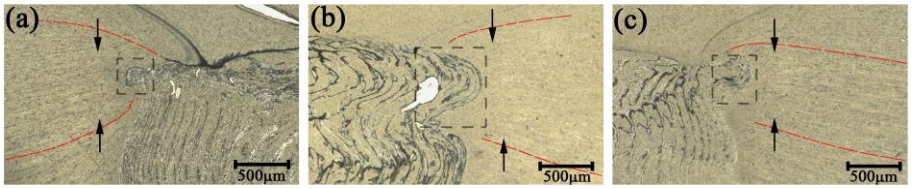

Figure 6

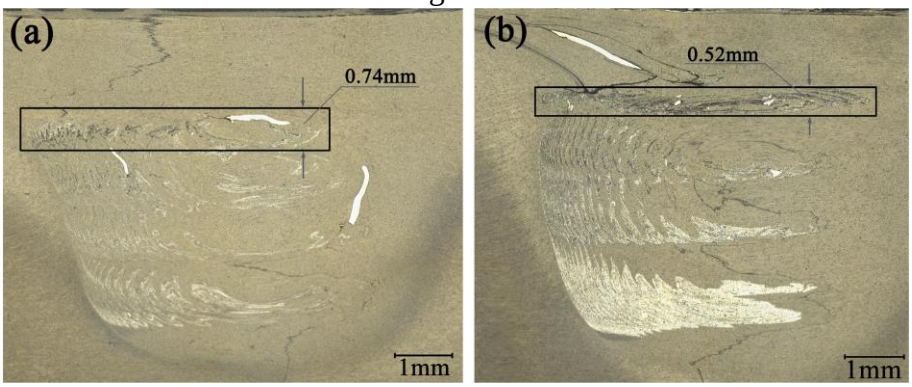

Figure 7

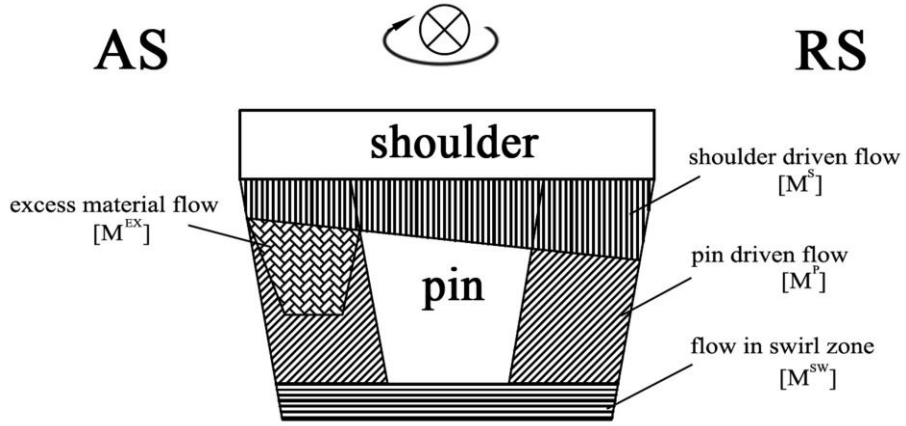

Figure 8

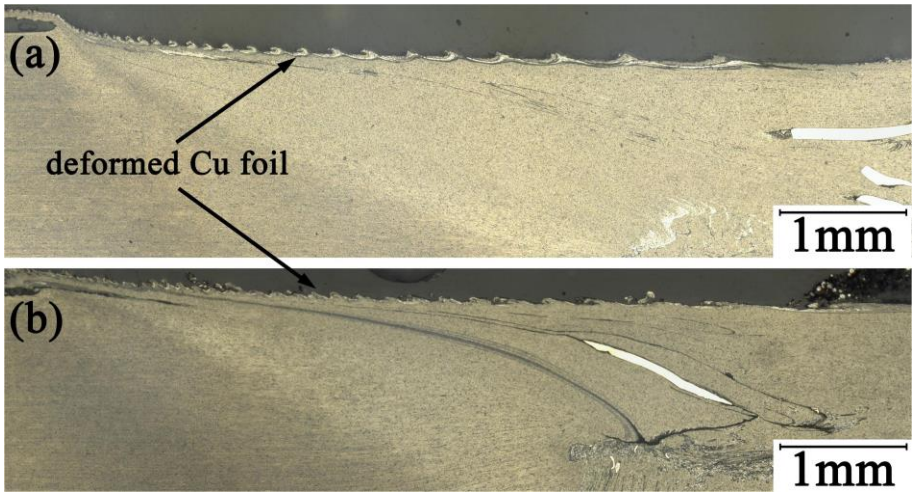

Figure 9

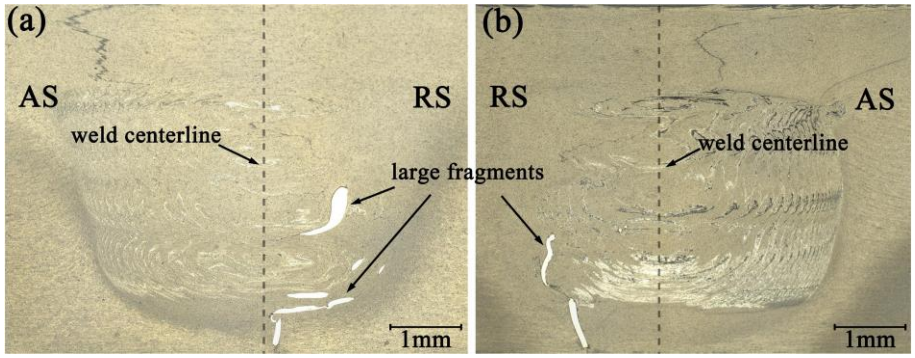

Figure 10

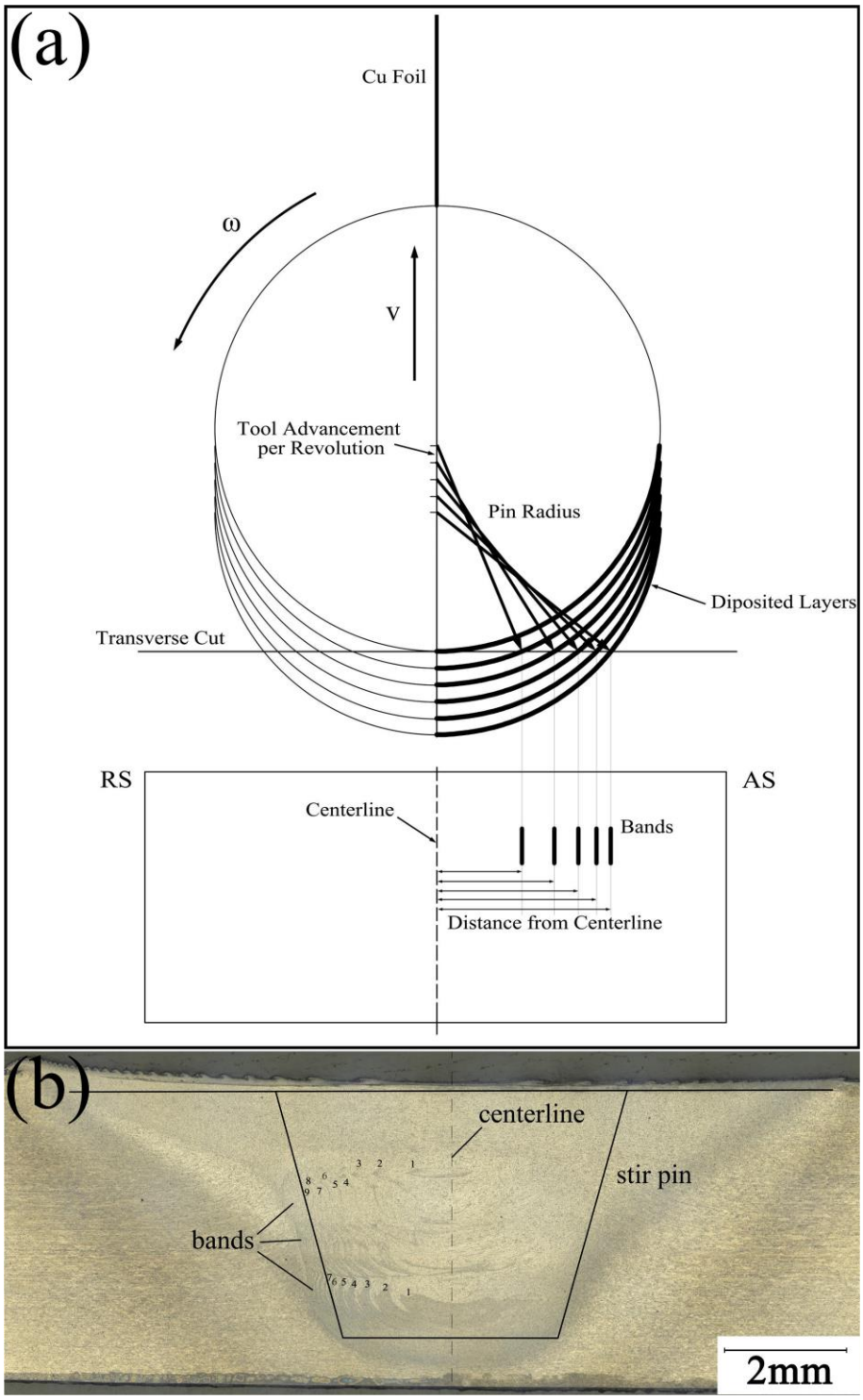
(a)
Cu Foil
ω
V
Tool Advancement
per Revolution
Pin Radius
Diposited Layers
Transverse Cut
RS
AS
Centerline
Bands
Distance from Centerline
(b)
centerline
stir pin
bands
2mm

Figure 11

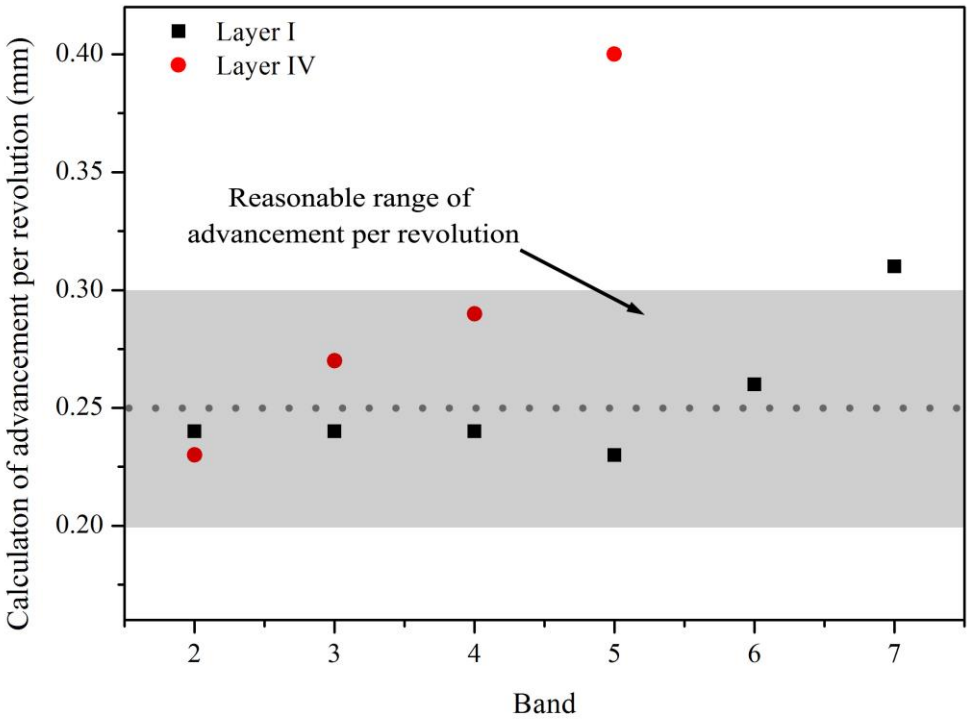

Figure 12

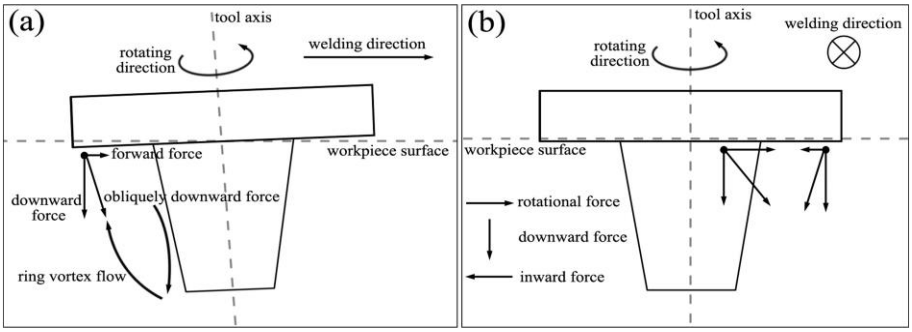

Figure 13